Supporting Information

Topology-Controlled Porous Carbons with Dispersed Cu Catalysts for Efficient Electrocatalytic Nitrate Reduction to Ammonia

Rui Qiao, [a] Manling Zhang, [a] Hongyin Hu, [a] Donghua Li, [a] Mingliang Du, [a,b] and Shuanglong Lu [a]*

[a]Key Laboratory of Synthetic and Biological Colloids, Ministry of Education, School of Chemical and Material Engineering, Jiangnan University, Wuxi, Jiangsu 214122, P. R. China. E-mail: lushuanglong@jiangnan.edu.cn

[b]Zhejiang Provincial Innovation Center of Advanced Textile Technology, Shaoxing 312000, China

Contents

1. Experimental section

Reagents. Hexakis (benzylthio) benzene (98%) was purchased from Xiangrui Technology Co., Ltd. (Nanjing, China). Thiophene (Guaranteed Reagent (GR)), chloroform (Analytical Reagent (AR)), ferric chloride ($FeCl_3$, anhydrous, AR), methanol (anhydrous, AR), ethanol (anhydrous, AR), cyclohexane (AR), potassium nitrate (KNO_3, AR), and $Cu(OAc)_2 \cdot H_2O$ (AR) were procured from Sinopharm Chemical Reagent Co., Ltd. (Shanghai, China). Potassium hydroxide (AR) was sourced from Titan Technology Co., Ltd. (Shanghai, China). Argon gas (Ar, 99.999%), nitrogen gas (N_2, 99.999%) and ammonia gas (NH_3, 99.999%) were obtained from Xinxiyi Technology Co., Ltd. (Wuxi, China). Nafion 117 membrane was obtained from Dupont Co., Ltd. (USA). Deionized water (resistivity: ca.18.42 MΩ cm) was used to prepare the electrolyte solutions. All reagents and solvents used in experiments were commercially available and were used without further purification.

Synthesis of NT and NS. 0.10 g of Hexakis (benzylthio) benzene and 10 μL of thiophene were added to a 150 ml flask. 50 mL of chloroform was added to dissolve the mixture, and N_2 was bubbled through as a protective atmosphere. The mixture was stirred at 25 ℃ for 30 minutes. Then, 0.57 g (3.5 mmol) of $FeCl_3$ was added, and the mixture was stirred under N_2 atmosphere for 0.5 hours to pre-polymerize. The mixture was then filtered to remove solid impurities, and the filtrate was transferred to a Teflon-lined autoclave. The autoclave was heated in an oven at 150 ℃ for 48 h. After cooling, the precipitate was collected by filtration. The solid was then purified by Soxhlet extraction with methanol for 72 h. Nanosheets (NS) were synthesized using the same procedure as NT, with the only difference being that the amount of chloroform used was reduced to 10 mL.

Synthesis of Cu@NT and Cu@NS. $Cu(OAc)_2 \cdot H_2O$ dissolved in ethanol to obtain a Cu^{2+} concentration of 1 mg ml^{-1} solution. 15 mg of NT was dispersed in 15 ml of ethanol, and then 100 μL of Cu^{2+} solution was added. Stirred at 25 °C under nitrogen protection for 24 h. After centrifugation, further addition of cyclohexane was freeze-dried overnight to obtain Cu@NT. Cu@NS and Cu@NT coordinate metal in exactly the same way.

Synthesis of NT-Cu, NT-Cu-NH_3 and NS-Cu-NH_3. Cu@NT was placed into a tube furnace, heating under Ar atmosphere at a rate of 2.5 °C min^{-1} to 1000 °C and maintain at this temperature for 3 h to obtain black powder, designated as NT-Cu. For comparison, heat Cu@NT first under Ar atmosphere for 2.5 h, followed by heating under a mixed atmosphere of Ar and NH_3 (volume ratio = 15:1) for 0.5 h to obtain NT-Cu-NH_3. Simultaneously, using Cu@NS as a precursor, NS-Cu-NH_3 was prepared under the same conditions.

Materials Characterization. The morphology and size of the samples were characterized using field-emission scanning electron microscopy (FE-SEM, Hitachi, Japan, S-4800) and transmission electron microscopy (TEM, JEOL, Japan, JEM-2100PLUS) at accelerating

voltages of 3 kV and 200 kV, respectively. X-ray photoelectron spectroscopy (XPS) was conducted on a Kratos Axis Supra spectrometer (Kratos, UK). X-ray diffraction (XRD) measurements were performed on a D8 Advance X-ray diffractometer (Bruker, Germany) using monochromatic Cu Kα radiation. Fourier transform infrared spectroscopy (FT-IR) was conducted using a Nicolet iS5 FTIR spectrometer (TMO, US). Morphological and elemental analyses were performed with a field-emission scanning transmission electron microscope (STEM, TMO, US, Talos F200X G2).

Electrochemical Measurements.

A total of 3 mg of the material was weighed and placed into a 2 mL sample vial, to which 970 μL of isopropanol and 30 μL of 5 wt% Nafion 117 solution were added. The mixture was ultrasonically dispersed for 30 minutes, resulting in a homogeneous catalyst ink. Subsequently, 50 μL of the catalyst ink was loaded onto a 1×1 cm^2 hydrophobic carbon paper and air-dried, resulting in a catalyst loading of 0.15 mg cm^{-2}.

All electrochemical measurements were performed using a conventional three-electrode system on an AUTOLAB PGSTAT302N electrochemical workstation. The working electrode was prepared using the catalyst-coated carbon paper, while a carbon rod was employed as the counter electrode, and a saturated calomel electrode (Hg/Hg_2Cl_2, SCE) was used as the reference electrode. Electrochemical nitrate reduction reaction (NO_3RR) tests were conducted in a two-compartment H-cell separated by a Nafion 117 proton exchange membrane, using 0.1 M KOH and 0.5 M KNO_3 as the electrolyte solutions. The tests included cyclic voltammetry (CV), linear sweep voltammetry (LSV), and chronoamperometry (i-t). All potentials mentioned in this study were converted to the reversible hydrogen electrode (RHE) scale using the equation:

$$E_{RHE} = E_{SCE} + 0.0591 \times pH + 0.197$$

Constant potential tests were conducted at intervals of −0.1 V within a potential range of −0.59 to −1.09 V vs. RHE, with each potential held for 1 hour under stirring at 400 rpm. Isotopic labeling experiments were performed at −0.99 V vs. RHE under identical conditions, except that the nitrogen source was replaced with 99% $K^{15}NO_3$.

The electrochemical surface area (ECSA) was determined by measuring CV curves at different scan rates within a non-Faradaic potential range. A plot of the non-Faradaic current density ($\Delta j = 0.5 \times |j_{charge} - j_{discharge}|$) against the scan rate produced a linear relationship, with the slope corresponding to the electrochemical double-layer capacitance (C_{dl}). The ECSA was calculated by dividing C_{dl} by the specific capacitance (C_S) of the sample.

Product concentration determination.

Ultraviolet-visible spectroscopy (UV-Vis) was employed for the quantitative detection of electrocatalytic products. The post-electrolysis electrolyte was diluted to an appropriate

concentration to fall within the range of the standard calibration curve, and a chromogenic agent was used for color development. The concentration of the products was then calculated based on the corresponding standard curve.

For the detection of NO_2^- , a chromogenic reagent consisting of p-aminobenzenesulfonamide (4 g), N-(1-naphthyl) ethylenediamine dihydrochloride (0.2 g), ultrapure water (50 mL), and phosphoric acid (10 mL, ρ=1.70 g/mL) was used. A specific volume of the electrolyte was extracted from the electrolysis cell and diluted to 2 mL to match the detection range of the standard curve. Subsequently, 40 L of the chromogenic reagent was added to the 2 mL solution and mixed thoroughly. The concentration of NO_2^- in the electrolyte after testing was calculated using the absorbance at 525 nm and the standard calibration curve.

For the quantification of NH_3, the salicylate method was employed, wherein NH_3 reacts with salicylate and hypochlorite to form indophenol blue. The chromogenic reagents consisted of sodium hypochlorite solution (0.05 M, ~4.5% active chlorine), sodium nitroprusside solution (1 wt%), and a salicylate-citrate-NaOH mixture (prepared by dissolving 5 g of salicylic acid and 5 g of sodium citrate in 100 mL of 1 M NaOH solution). A specific volume of the electrolyte was extracted from the electrolysis cell and diluted to 2 mL. Subsequently, 400 μL of the salicylate-citrate-NaOH mixture, 200 μL of the sodium hypochlorite solution, and 200 μL of the sodium nitroprusside solution were sequentially added and mixed thoroughly. The solution was left to stand for 2 hours before UV-Vis measurement. The concentration of NH_3 in the electrolyte after testing was determined based on the absorbance at 658 nm and the corresponding standard calibration curve.

Calculation of Faradaic Efficiency (FE).

The Faradaic efficiency (FE) for the formation of each product was calculated according to the following equation:

$$FE = \frac{n \cdot F \cdot C \cdot V}{Q} \times 100\%$$

where n is the number of electrons transferred per molecule of product formed. According to the electrochemical reaction pathways, n equals 8 for the reduction of NO_3^- to NH_3, 2 for the reduction of NO_3^- to NO_2^-, and 2 for the hydrogen evolution reaction (HER, $H^+ \rightarrow H_2$). F is the Faraday constant (96485 C mol^{-1}). C (mol L^{-1}) is the concentration of the target product in the electrolyte, quantified by UV-vis spectroscopy (for NH_3 and NO_2^-) or gas chromatography (for H_2). V is the electrolyte volume, fixed at 0.05 L in this work. Q (C) is the total charge passed during the chronoamperometric test under a constant applied potential.

Calculation of NH_3 Yield Rate.

The NH_3 yield rate was calculated using the following equation:

$$\text{Yield Rate} = \frac{C \cdot V}{m \cdot t}$$

where C (mol L^{-1}) is the experimentally determined NH_3 concentration obtained from UV-vis calibration, V is the electrolyte volume (0.05 L), m is the catalyst loading on the working electrode (1.5×10^{-4} g), and t is the electrolysis time, fixed at 1 h in this study. The calculated yield rate is expressed in units of mol $g^{-1}_{catalyst}$ h^{-1}.

As an example, for NT-Cu-NH_3 at −0.99 V *vs.* RHE, the chronoamperometric test was conducted for 1 h. After electrolysis, the electrolyte was diluted by a factor of 80, and the NH_3 concentration determined by the indigo carmine method was 149.138 μmol L^{-1}. The actual NH_3 concentration in the electrolyte was therefore calculated to be 0.01193 mol L^{-1}. Substituting these values into the above equation gives:

$$Yield\ Rate = \frac{0.01193 \times 0.05}{1.5 \times 10 - 4 \times 1} = 3.98 \text{ mol g - 1 h - 1}$$

which agrees well with the reported average NH_3 yield of approximately 4.05 mol g^{-1} h^{-1}.

During the corresponding electrolysis, the catalyst exhibited an average current density of approximately 143.4 mA cm^{-2} (absolute value) over a geometric electrode area of 1 cm^2. This value was obtained by averaging the steady-state current density in the time window from 600 to 3600 s during the chronoamperometric test, thereby excluding the initial transient current response. The total charge passed (Q) was determined by integrating the steady-state current over the entire 1 h electrolysis period, yielding a value of 524.34 C.

2. Supporting Figures and Table

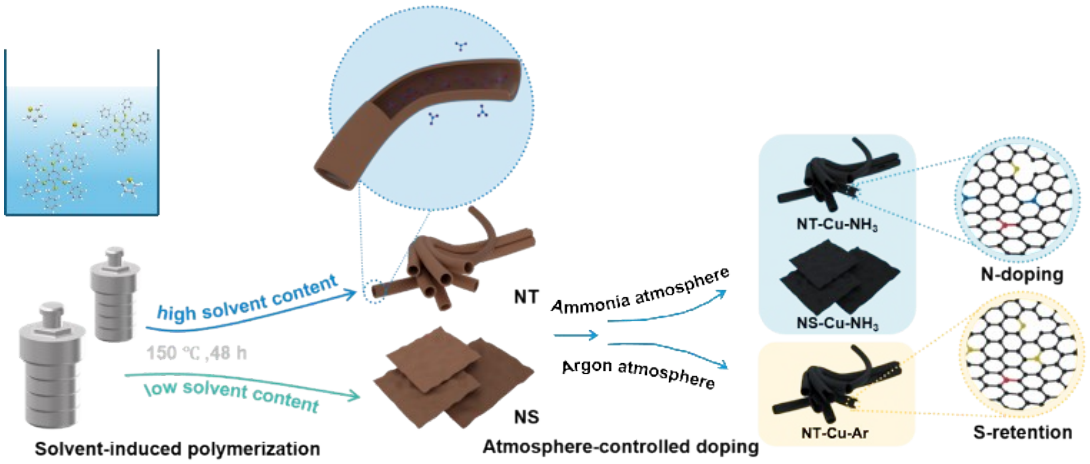

Fig. S1. Schematic diagram of NT-Cu-NH_3, NS-Cu-NH_3 and NT-Cu-Ar synthesis.

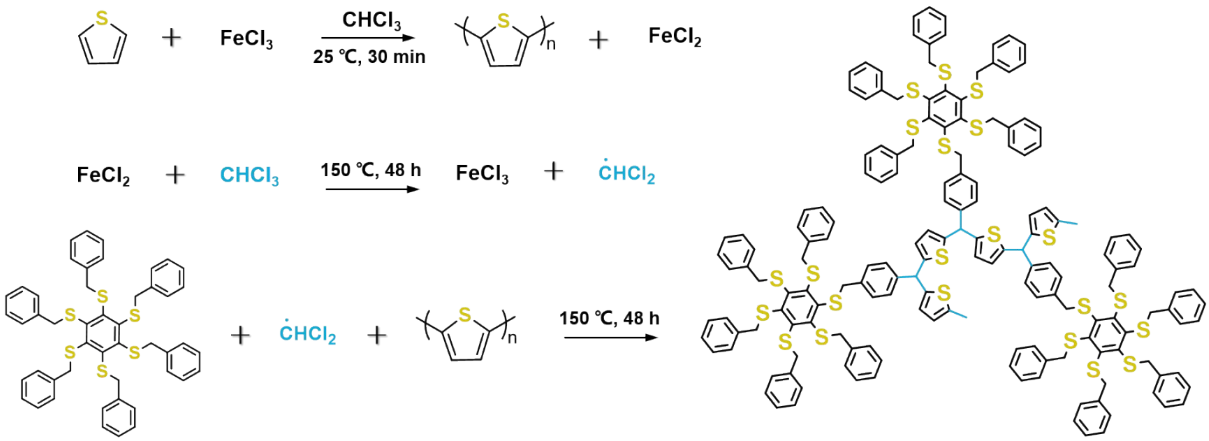

Fig. S2. Reaction mechanism of solvent-induced polymerization strategy.

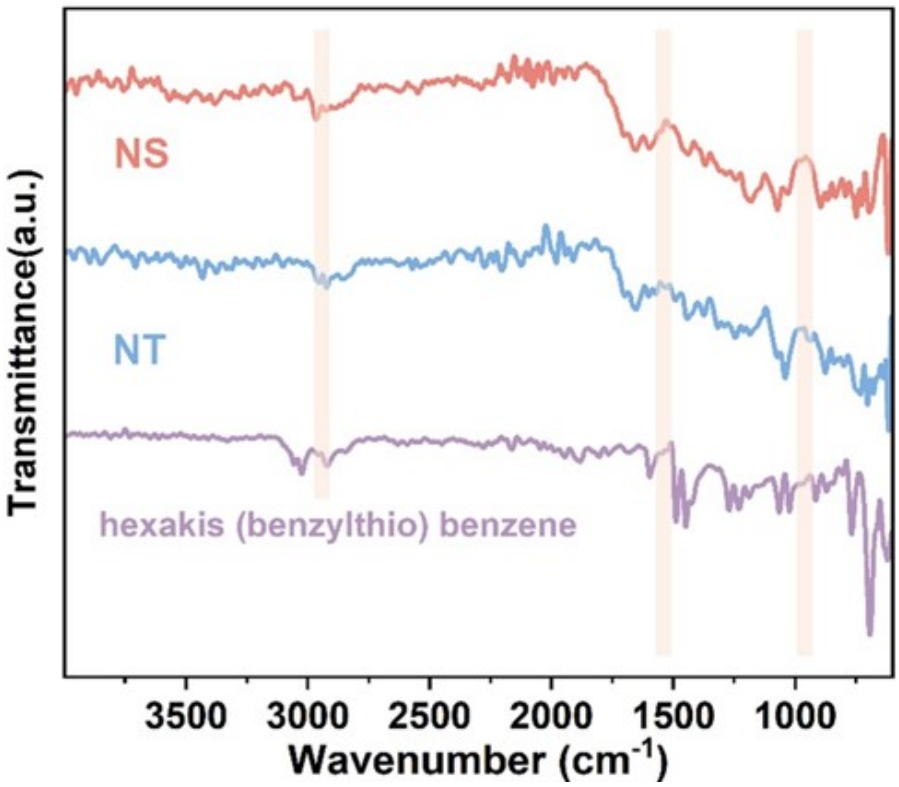

Fig. S3. FT-IR spectra of NT, NS and hexakis(benzylthio)benzene.

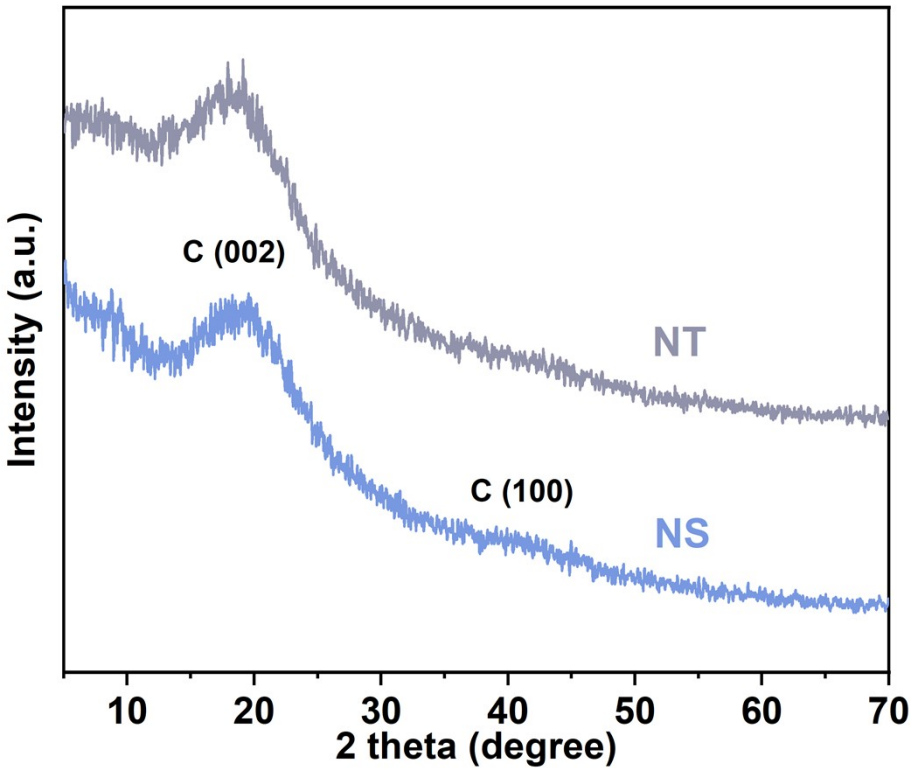

Fig. S4. XRD patterns of NT and NS.

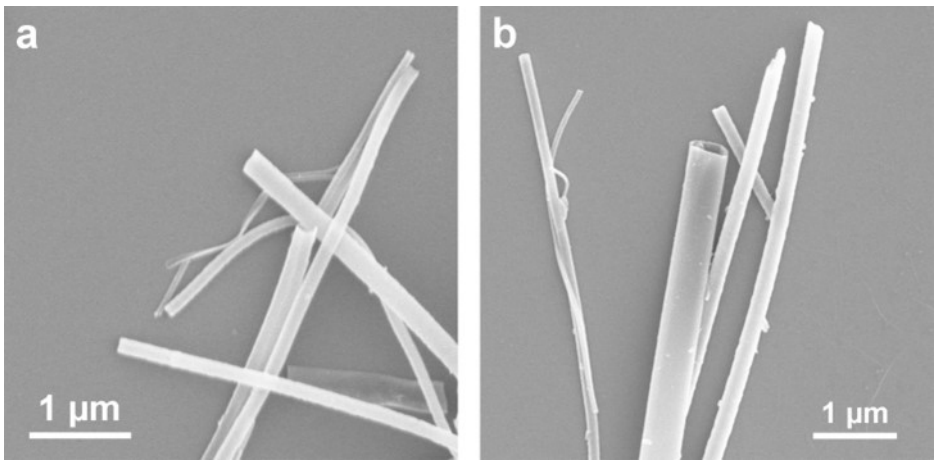

Fig. S5. SEM images of NT-Cu-Ar.

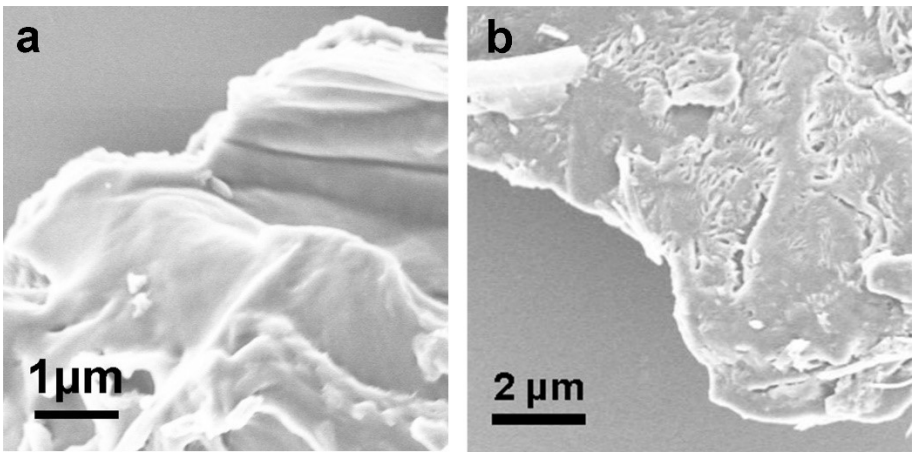

Fig. S6. SEM images of NS-Cu-NH_3.

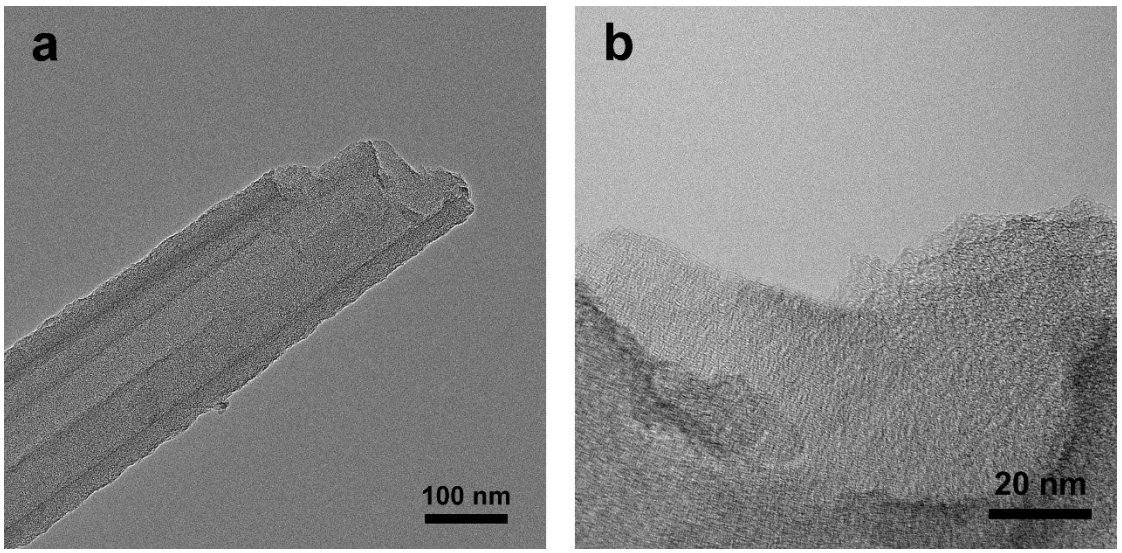

Fig. S7. TEM image of NT-Cu-Ar.

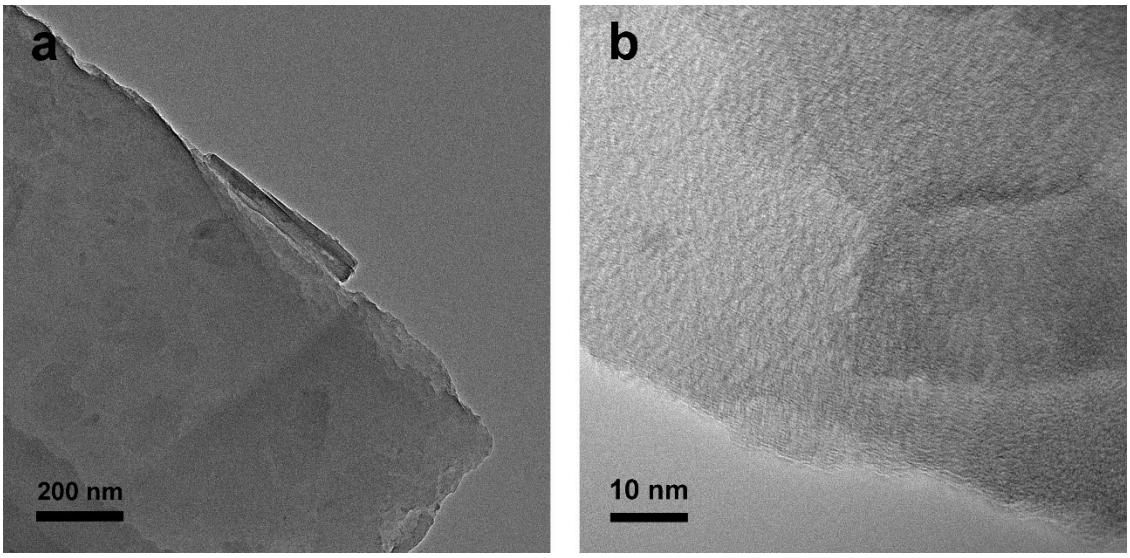

Fig. S8. TEM image of NS-Cu-NH_3.

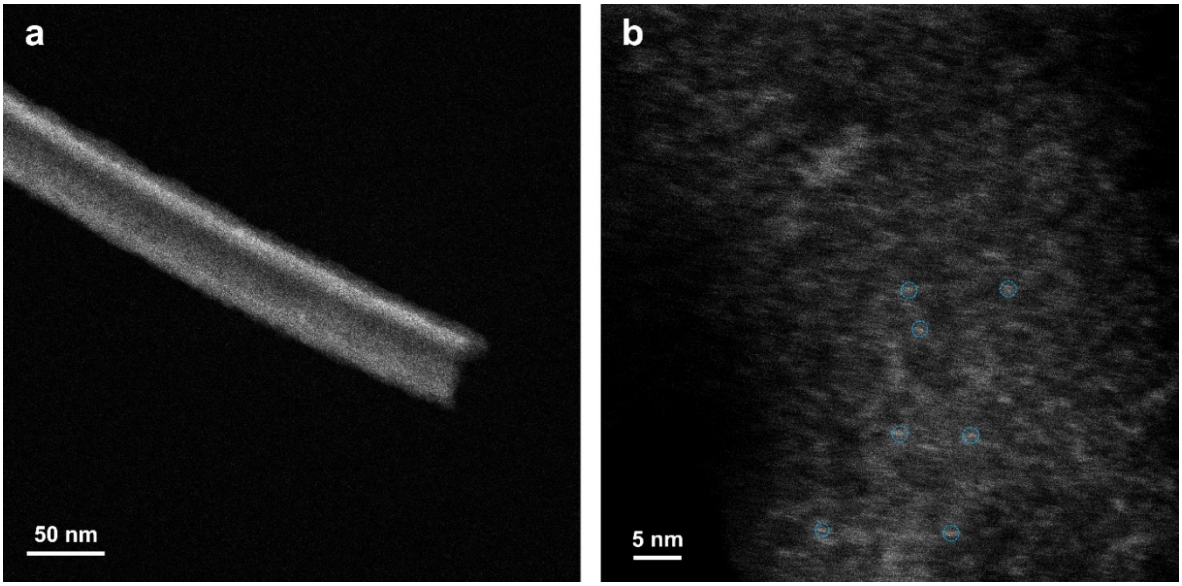

Fig. S9. Aberration-corrected HAADF-STEM image of NT-Cu-NH_3.

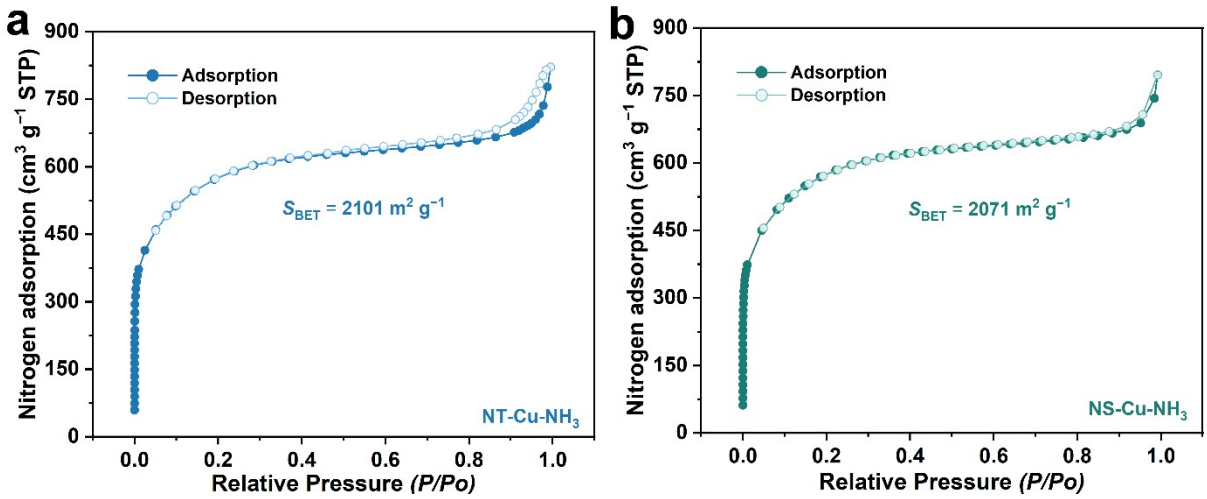

Fig. S10. N_2 sorption isotherms of (a) NT-Cu-NH_3 and (b) NS-Cu-NH_3.

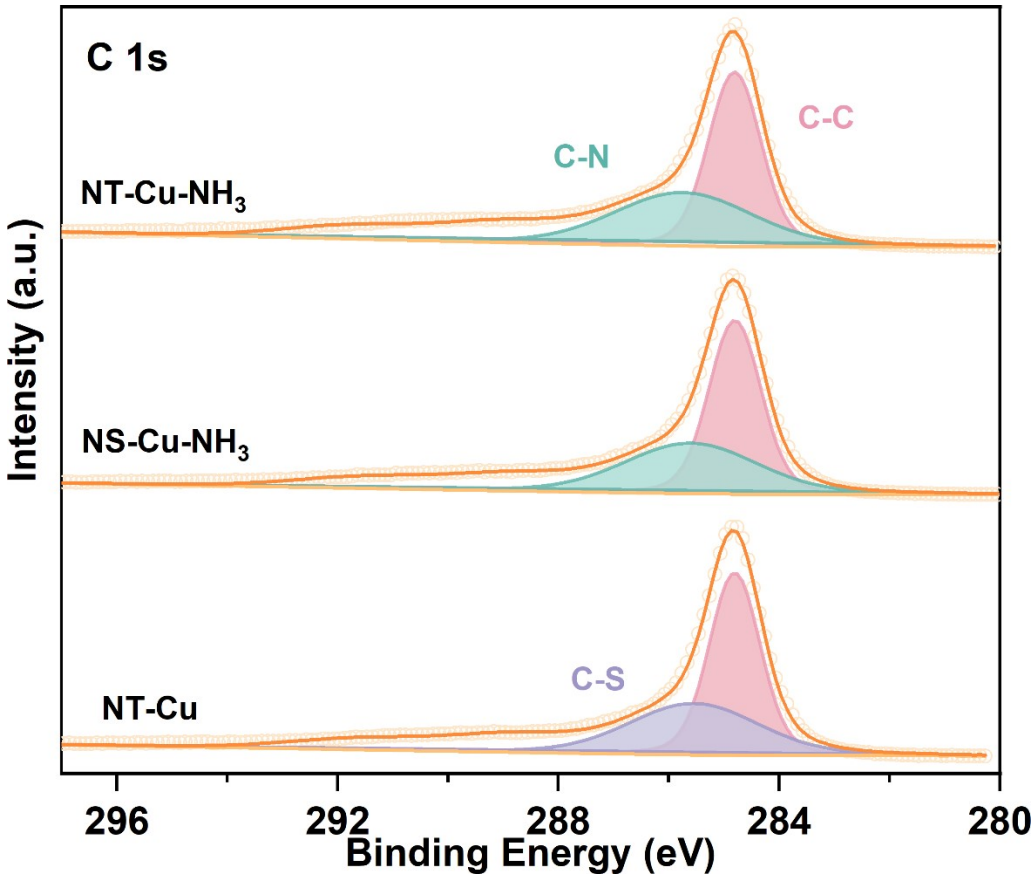

Fig. S11. High-resolution C1s XPS spectra of NT-Cu-NH_3, NS-Cu-NH_3 and NT-Cu-Ar.

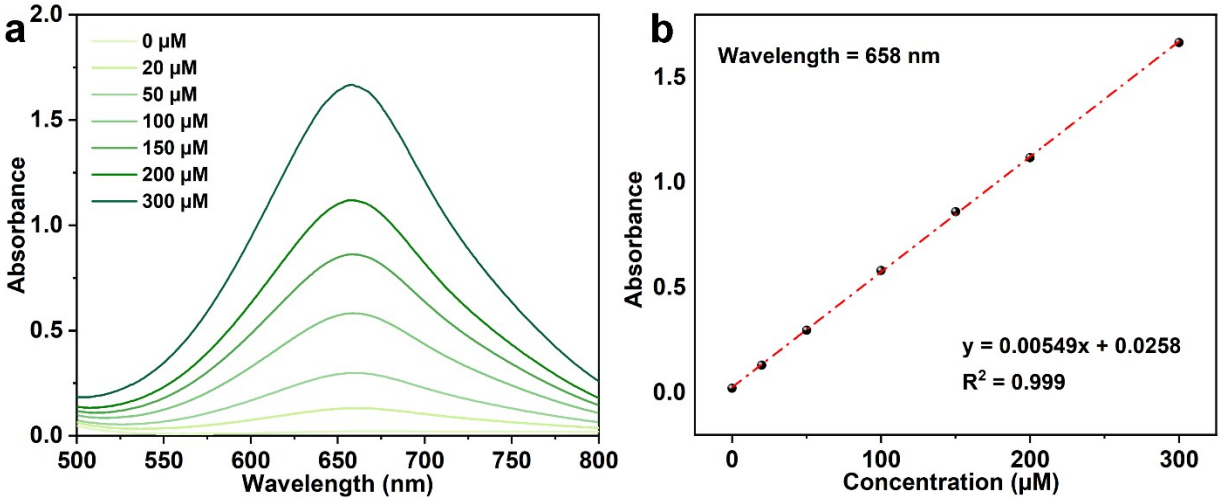

Fig. S12. The (a)UV-Vis curves and (b)calibration curves of the electrolyte with the given NH_3 concentrations.

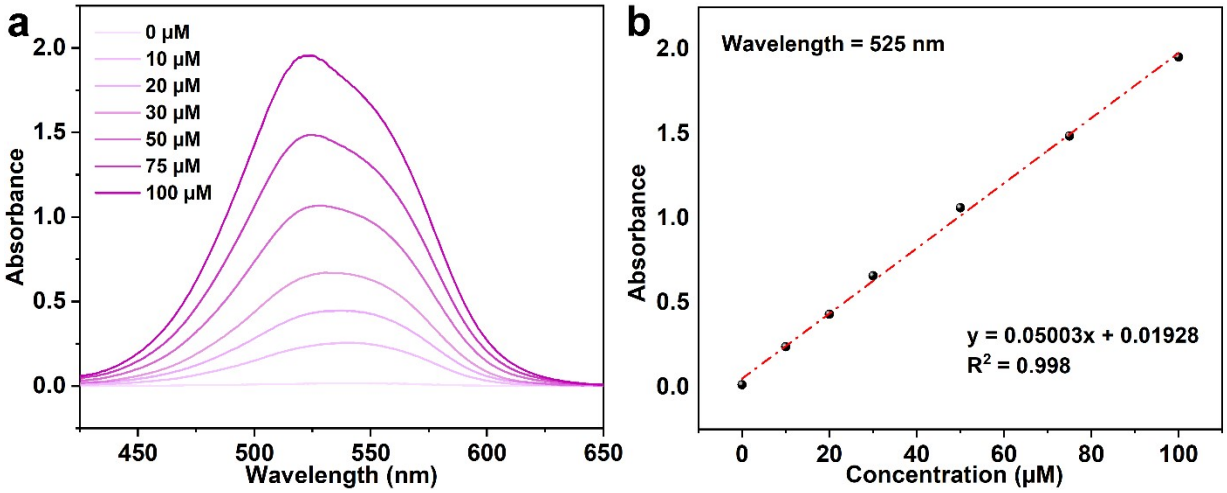

Fig. S13. The (a)UV-Vis curves and (b)calibration curves of the electrolyte with the given NO_2^- concentrations.

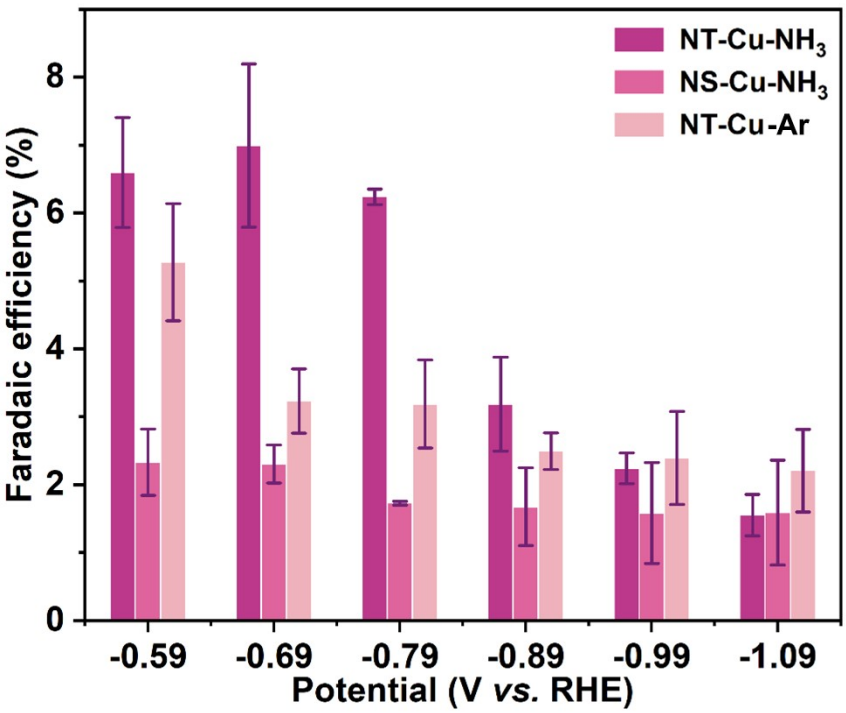

Fig. S14. NO_2^- FE of NT-Cu-NH_3, NS-Cu-NH_3 and NT-Cu-Ar at each given potential.

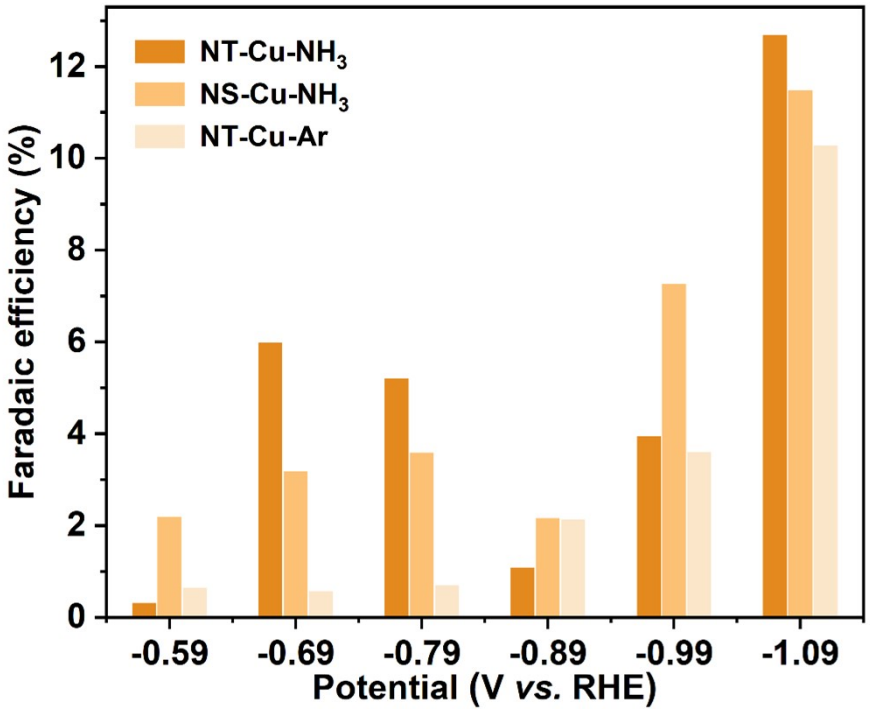

Fig. S15. H_2 FE of NT-Cu-NH_3, NS-Cu-NH_3 and NT-Cu-Ar at each given potential.

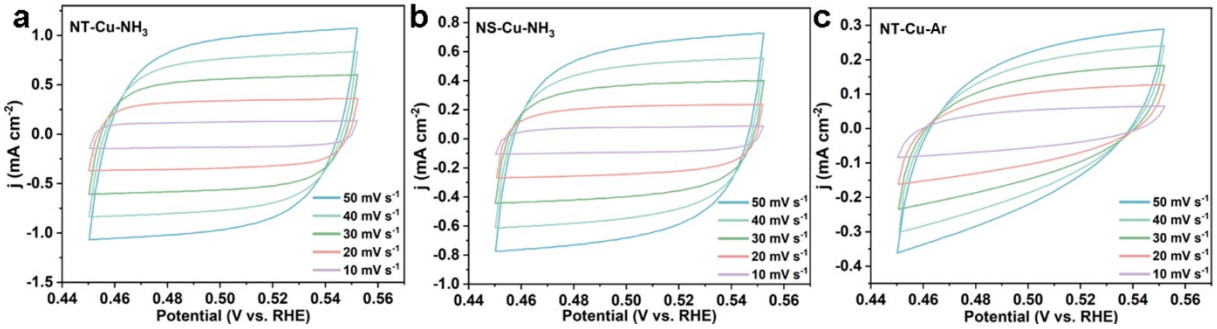

Fig. S16. CV with different scan rate for (a)NT-Cu-NH_3, (b)NS-Cu-NH_3 and (c)NT-Cu-Ar.

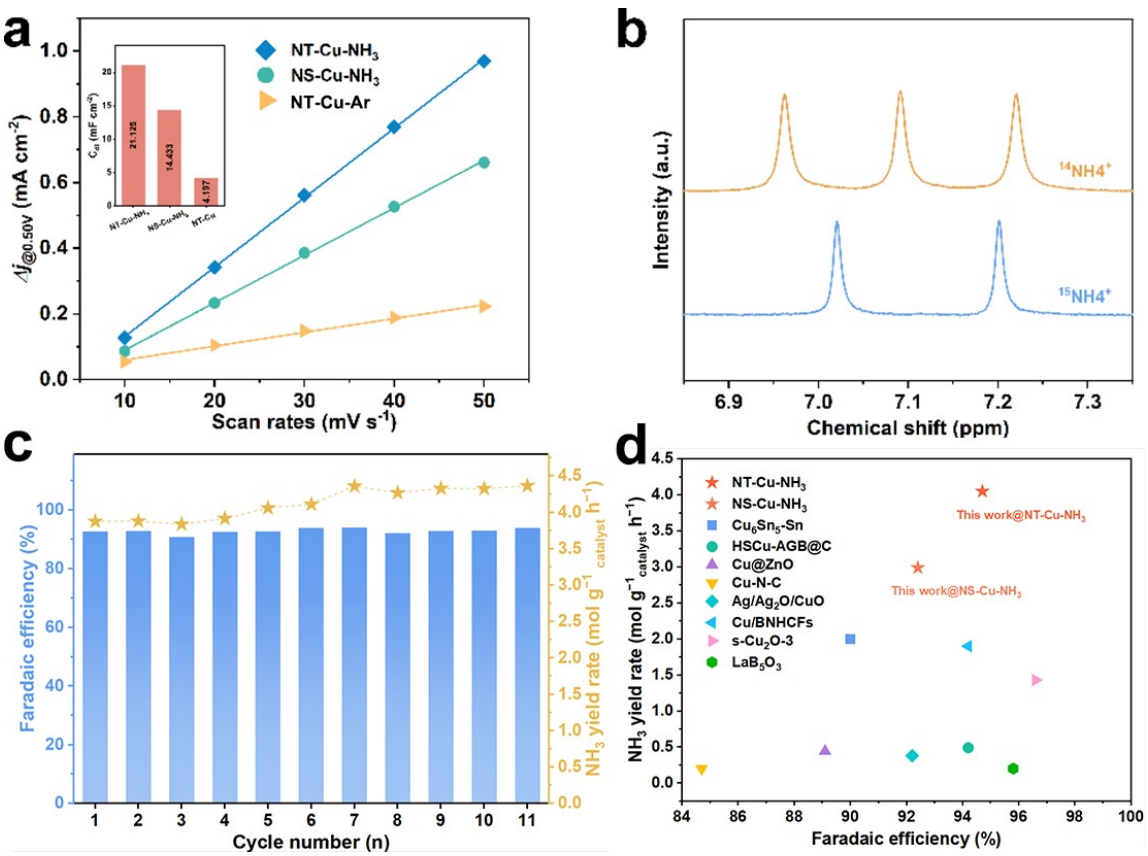

Fig. S17. (a) Double-layer capacitances of NT-Cu-NH_3, NS-Cu-NH_3, and NT Cu-Ar; (b) ^{1}H NMR spectrum of the electrolyte after testing NT-Cu-NH_3 at −0.99 V *vs.* RHE; (c) Cycling tests of NT-Cu-NH_3 for nitrate reduction at −0.99 V *vs.* RHE; (d) Comparison of NH_3 yield rate and FE between NT-Cu-NH_3, NS Cu-NH_3, and other Cu-based electrocatalysts for NO_3RR.

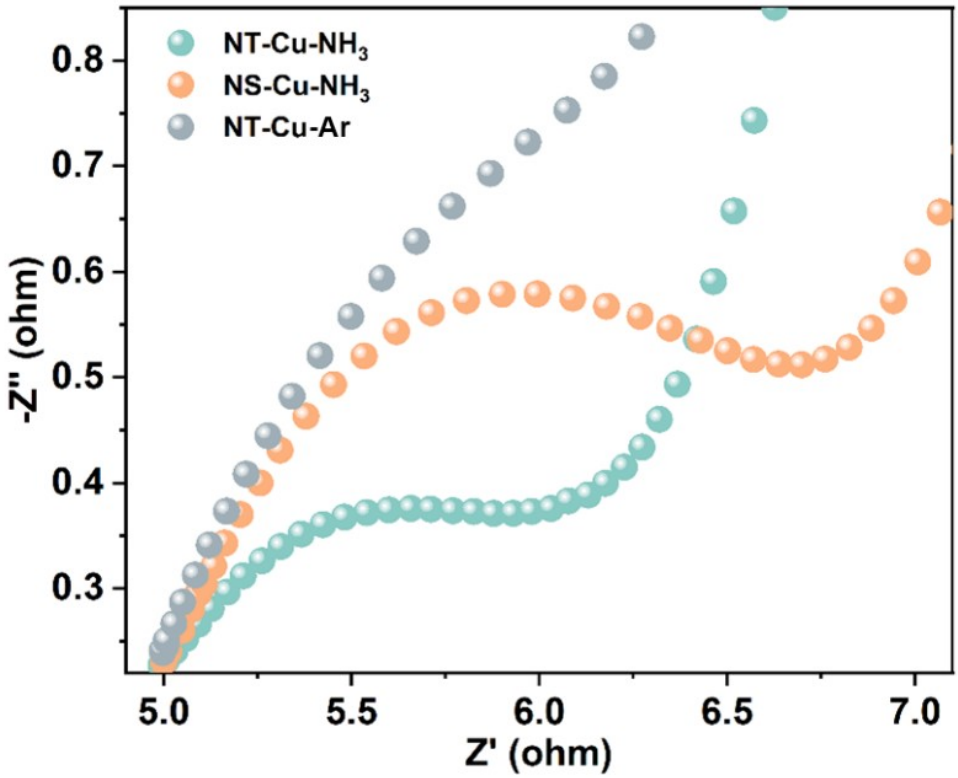

Fig. S18. EIS image of NT-Cu-NH_3, NS-Cu-NH_3 and NT-Cu-Ar.

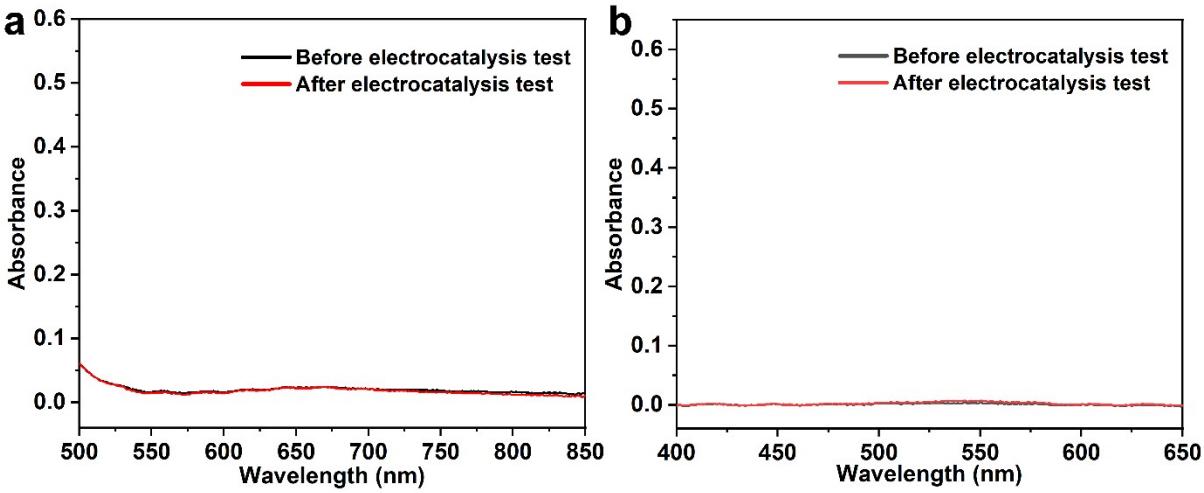

Fig. S19. UV-Vis curves of electrolytes before and after electrocatalysis test for NT-Cu-NH_3 in a KOH solution without KNO_3. (a) UV-vis curves for NH_3; (b) UV-vis curves for NO_2^-.

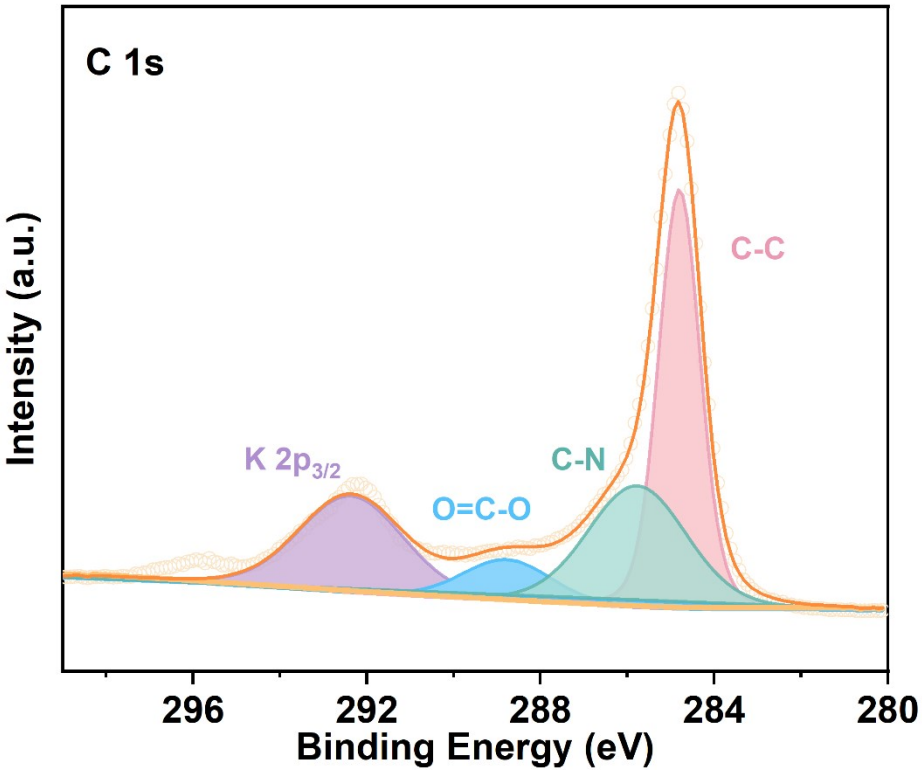

Fig. S20 High-resolution C1s XPS spectra of NT-Cu-NH_3 after test.

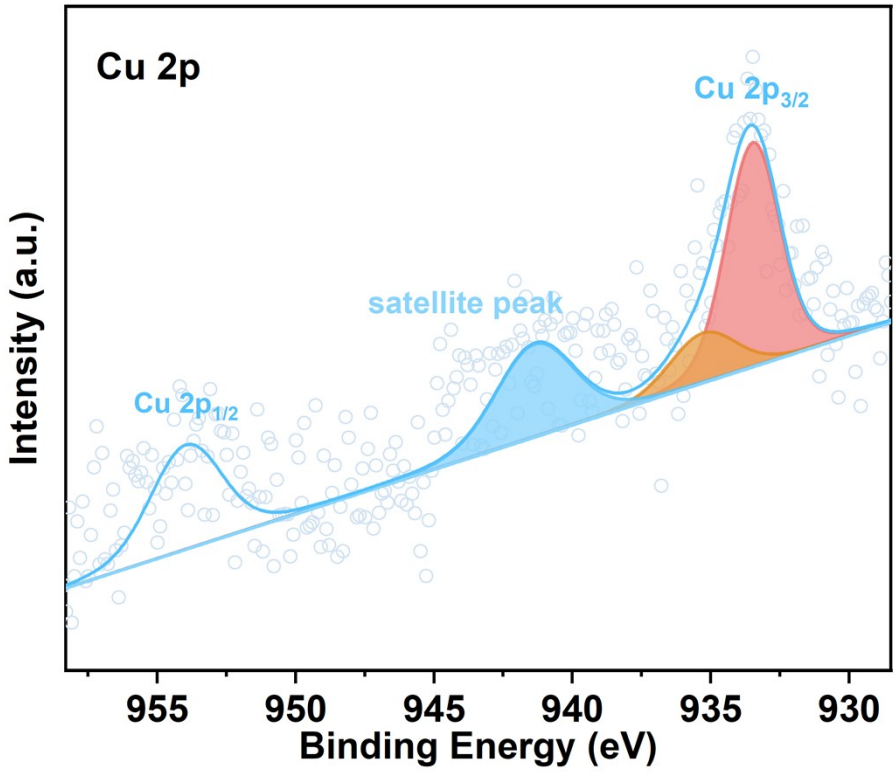

Fig. S21. High-resolution Cu2p XPS spectra of NT-Cu-NH_3 after test.

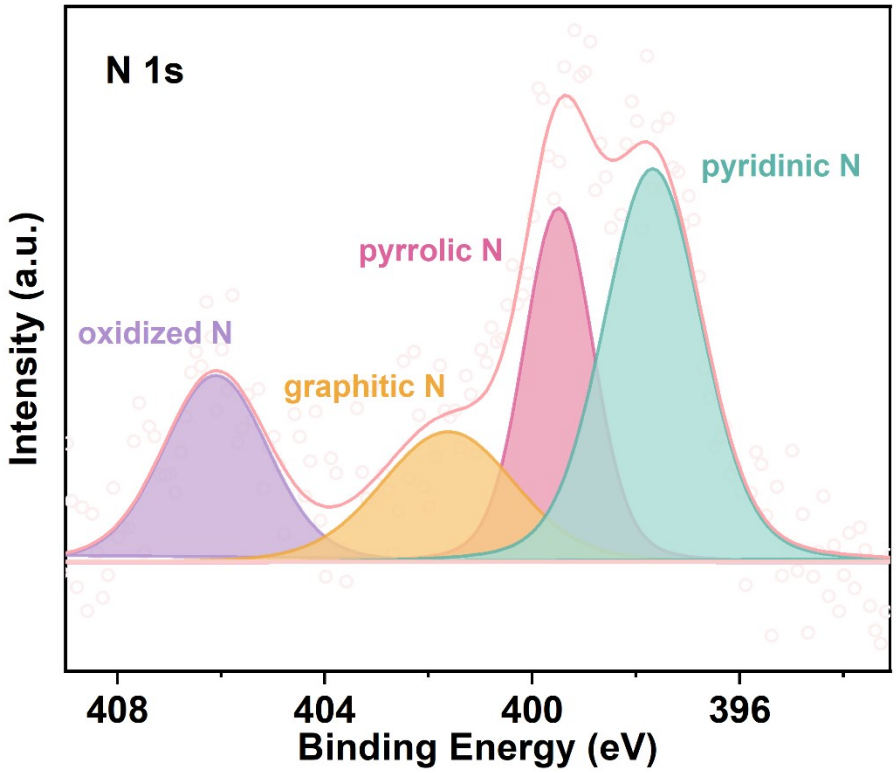

Fig. S22. High-resolution N1s XPS spectra of NT-Cu-NH_3 after test.

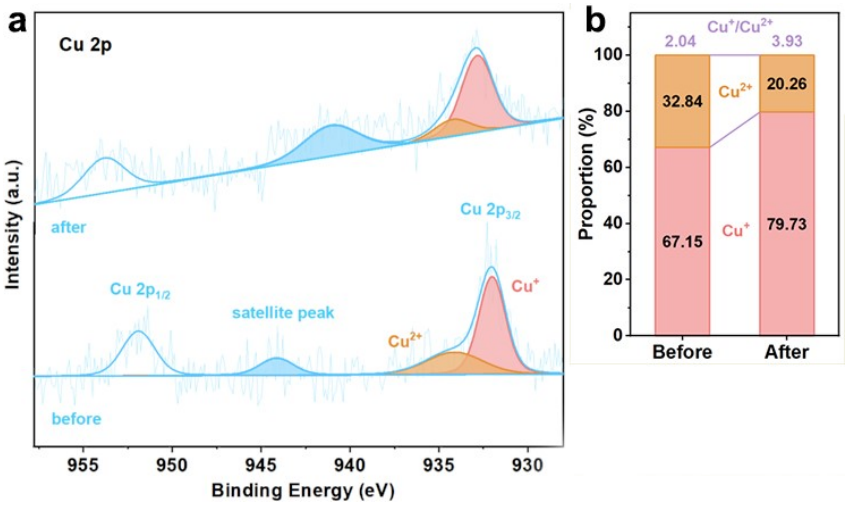

Fig. S23. (a) High-resolution Cu 2p XPS spectra of NT-Cu-NH_3 before and after test. (b) Comparison of Cu valence state distribution derived from XPS peak deconvolution before and after electrochemical cycling, highlighting the increased proportion of Cu^+ species after long-term NO_3RR operation.

Table S1. Summary of recently reported NH_3 yield rate and Faraday efficiencies for copper-doped catalyst performance.

electrocatalyst	NH_3 yield rate (mol g^{-1} h^{-1})	NH_3 yield rate (mol cm^{-2} h^{-1})	Faraday efficiency (%)	Electrolyte	Catalyst loading (g)	testing time (h)	Ref.
NT-Cu-NH_3	4.05	6.08×10^{-4}	94.7	0.1 M KOH	1.5×10^{-4}	1.0	This work
NS-Cu-NH_3	2.99	4.49×10^{-4}	92.4	(0.5 M KNO_3)	1.5×10^{-4}	1.0	This work
Cu_6Sn_5-Sn NPs	2.00	2.00×10^{-4}	90.0	0.1 M KOH (0.1 M KNO_3)	1×10^{-4}	2.0	[1]
HSCu-AGB@C	0.49	9.76×10^{-4}	94.2	1 M KOH (0.1 M KNO_3)	5×10^{-4}	1.0	[2]
CuCo-TPA-E	–	1.12×10^{-3}	99.6	1 M KOH (0.1 M KNO_3)	–	0.5	[3]
NiBDC@HsGDY@Cu	–	3.20×10^{-4}	99.2	1 M KOH (0.1 M NO_3^-)	–	1.0	[4]
$Cu_{50}Ni_{50}$	–	5.84×10^{-4}	89.6	1 M KOH (0.1 M KNO_3)	–	2.0	[5]
Cu@ZnO NWA	0.44	3.55×10^{-4}	89.1	0.1 M KOH (0.1 M KNO_3)	8×10^{-4}	2.0	[6]
Cu-N-C SAC	0.20	2.65×10^{-4}	84.7	0.1 M KOH (0.1 M KNO_3)	8×10^{-3}	0.5	[7]
$Cu_{30}Co_{70}$	–	3.02×10^{-4}	~100	1 M KOH (0.1 M KNO_3)	–	1.0	[8]
Ag/Ag_2O/CuO	0.38	3.76×10^{-4}	92.2	1 M KOH (0.1 M KNO_3)	1×10^{-3}	1.0	[9]
Cu/BNHCFs	1.90	4.75×10^{-4}	94.2	1 M KOH (0.1 M KNO_3)	2.5×10^{-4}	1.0	[10]
s-Cu_2O-3	1.43	2.85×10^{-4}	96.6	1 M KOH (0.1 M KNO_3)	5×10^{-5}	0.5	[11]
LaB_5O_3	0.20	2.97×10^{-4}	95.8	1 M KOH (0.1 M KNO_3)	1.45×10^{-3}	1.0	[12]

References

1 J. Yu, A. F. Kolln, D. Jing, J. Oh, H. Liu, Z. Qi, L. Zhou, W. Li, W. Huang, ACS Appl. Mater. Interfaces, 2021, 13, 52073-52081.

2 Q. Hu, Y. Qin, X. Wang, H. Zheng, K. Gao, H. Yang, P. Zhang, M. Shao, C. He, CCS Chemistry, 2022, 4, 2053-2064.

3 J. Yang, W. Zhang, H. Zhao, Y. Zou, Z. Zhang, J. Liu, J. Wang, Z. Gu, X. Yan, Appl. Catal. B-Environ.,2024, 340, 123237.

4 B. Wang, J. Ma, R. Yang, B. Meng, X. Yang, Q. Zhang, B. Zhang, S. Zhuo, Angew. Chem., Int. Ed., 2024, 63, e202404819.

5 Y. Bu, C. Wang, W. Zhang, X. Yang, J. Ding, G. Gao, Angew. Chem., Int. Ed., 2023, 62, e202217337.

6 A. Feng, Y. Hu, X. Yang, H. Lin, Q. Wang, J. Xu, A. Liu, G. Wu, Q. Li, ACS Catal., 2024, 14, 5911.

7 J. Yang, H. Qi, A. Li, X. Liu,X. Yang, S. Zhang, Q. Zhao, Q. Jiang, Y. Su, L. Zhang, J. Li, Z. Tian, W. Liu, A. Wang, T. Zhang, J. Am. Chem. Soc, 2022, 144: 12062-12071.

8 A. Wu, Y. Zhou, J. Lv, D. Zhang, Y. Peng, Q. Ye, P. Fu, W. Wang, X. Lin, S. Liu, M. Xu, Z. Qi, S. Zhu, W. Zhu, J. Yan, X. Tu, X. Li, ACS Sustainable Chem. Eng., 2022, 10, 14539-14548.

9 W. Go, R. A. Senthil, J. Cherusseri, A. Kumar, C. J. Moon, W. Limphirat, M. Ubaidullah, M. Y. Choi, Adv. Funct. Mater, 2025, 35, e11876.

10 R. He , L. Sun , K. Ren , X. Li , P. Tian , J. Ye, J. Mater. Chem. A, 2026, 14, 394-402.

11 J. Li , K. Wu , J. Heng , L. Zhu , X. Wang , Q. Han , T. Qiang, Small, 2025, 21, 2411005.

12 L. Zhou , D. Feng , Z. Li , H. Li , C. Ge , X. Zhang , T. Ma, Adv. Funct. Mater, 2025, e14375.